

Spin relaxation in inhomogeneous quantum dot arrays studied by electron spin resonance

A. F. Zinovieva,* N. P. Stepina, A. I. Nikiforov, A. V. Nenashev, and A. V. Dvurechenskii
Institute of Semiconductor Physics, SB RAS, 630090 Novosibirsk, Russia

L. V. Kulik
Institute of Chemical Kinetics and Combustion, SB RAS, 630090 Novosibirsk, Russia

N. A. Sobolev and M. C. Carmo
Departamento de Física e I3N, Universidade de Aveiro, Aveiro, Portugal
 (Dated: January 17, 2021)

Electron states in a inhomogeneous Ge/Si quantum dot array with groups of closely spaced quantum dots were studied by conventional continuous wave (*cw*) ESR and spin-echo methods. We find that the existence of quantum dot groups allows to increase the spin relaxation time in the system. Created structures allow us to change an effective localization radius of electrons by external magnetic field. With the localization radius close to the size of a quantum dot group, we obtain fourfold increasing spin relaxation time T_1 , as compared to conventional homogeneous quantum dot arrays. This effect is attributed to averaging of local magnetic fields related to nuclear spins ^{29}Si and stabilization of S_z -polarization during electron back-and-forth motion within a quantum dot group.

PACS numbers: 73.21.La, 03.67.Lx, 72.25.Rb

Introduction

Electron spins in quantum dots (QDs) can be considered as promising candidates for realization of quantum computation ideas and spintronics devices.^{1,2} The main parameter indicating the applicability of a system for quantum computation is the spin coherence time. An extremely long spin lifetime is observed in zero-dimensional structures due to a strong confinement in all three dimensions.³ An especially great potential for a long coherence time is expected in the Ge/Si system with quantum dots. In this system electrons are localized in strained Si regions, where spin-orbit (SO) coupling is very weak. However, recent investigations of spin decoherence by spin echo method in the Ge/Si QD system⁴ demonstrated that the spin relaxation times are unexpectedly short ($\sim 10\mu\text{s}$). It was suggested that the reason of such intensive spin relaxation consists in the appearance of effective magnetic fields during electron tunneling between quantum dots. These magnetic fields (Rashba fields)⁵ originate from spin-orbit interaction and arise due to the absence of mirror symmetry of the localizing potential for an electron in the vicinity of Ge QD. Spin relaxation occurs through stochastic spin precession in effective magnetic fields during random tunneling between QDs (analog of Dyakonov-Perel mechanism for delocalized carriers⁶). Obviously, suppression of the tunneling in the array of well-separated quantum dots allows to eliminate the existence of in-plane fluctuating magnetic fields. In this case the hyperfine interaction with ^{29}Si nuclear spins comes into force and determines the spin relaxation time. If the tunneling is suppressed not by spatial separation of QDs, but by Coulomb repulsion⁷, the anisotropic exchange interaction can also control the

spin relaxation process.

The efficiency of each mechanism depends in different ways on the localization degree of electrons. Changing the tunnel coupling between quantum dots (by changing their density) and correspondingly, the localization degree of electrons, it is possible to alter the relative contribution of different mechanisms. With the increase of electron localization radius the contribution of hyperfine interaction becomes smaller due to averaging-out of different orientations of nuclear spins. A related increase of the relaxation time occurs until the moment when the wave function overlapping provides the hopping between neighboring localization centers. In these conditions Dyakonov-Perel mechanism begins to control the spin relaxation process.⁸ Longest spin relaxation time is expected right before the point where Dyakonov-Perel mechanism comes into force. Similar effect was detected for n-type GaAs impurity system, where threefold increase of spin relaxation time was obtained in the vicinity of metal-to-insulator transition.⁹

In self-assembled tunnel-coupled QD structures it is hard to get a gradual change of the localization radius by changing the QD array density. The stochastic nucleation of QDs during growth in Stranskii-Krastanov mode¹⁰ leads to the formation of the regions with a high local density of QDs. In such regions a strong tunnel coupling between dots results in the intensive spin relaxation through Dyakonov-Perel mechanism. However, under certain conditions, the existence of groups of closely located QDs can provide not a decrease, but an increase of the spin relaxation time. First, QD groups should be well separated from each other. In this case, the effective magnetic fields can be averaged due to electron back-and-forth motion within each QD group. Second, QDs

inside the group should have strong tunnel coupling providing the effective localization radius comparable with QD group size. As a result, the averaging of local magnetic fields related to nuclear spins will take place.

The present work is devoted to the electron spin resonance (ESR) study of inhomogeneous QD arrays, where the averaging of Rashba and hyperfine fields inside QD groups is expected to provide a long spin relaxation time. We succeed in creating the experimental structure containing well separated groups of QDs with a large electron localization radius. The coupling between QDs and, consequently, the electron localization radius in the structures under study turned out to be dependent on the external magnetic field orientation. A fourfold increase of the spin relaxation time as compared to the previous data for dense homogeneous QD arrays⁴ has been detected at a special orientation of magnetic field, where the electron localization radius was close to the QD group size.

I. SAMPLES AND EXPERIMENT

The samples were grown by molecular-beam epitaxy on n-Si(001) substrates with the resistivity of 1000 Ω cm. To increase the response from the sample, we have grown 6 layers of the Ge nanoclusters separated by 30 nm Si-layers. Each QD layer was formed by deposition of 7 ML Ge at the temperature $T = 550^\circ\text{C}$. On the top of the structure, a $0.3\ \mu\text{m}$ epitaxial n-Si layer (Sb concentration $\geq 10^{17}\text{cm}^{-3}$) was grown, the same layer was formed below QD layers. The scanning tunneling microscopy (STM) of the structure with a single QD layer uncovered by Si shows the bimodal distribution of QDs (*hut*- and *dome*-clusters) (Fig. 1). The density of *dome*-clusters is $\sim 10^{10}\text{cm}^{-2}$, the typical base width is $l = 50\text{nm}$, the height is $h = 10\text{nm}$. The *hut*-clusters are distributed between *dome*-clusters with density $\sim 10^{11}\text{cm}^{-2}$, their typical base width is $l = 15\text{nm}$, the height is $h = 1.5\text{nm}$.

The obtained sizes of *dome*-clusters have to provide a strong localization of electrons at the apex of such type QDs with a small localization radius. To increase the localization radius, we used the temperature 500°C for overgrowth of QDs allowing to transform *dome*-clusters to disk-like clusters without intensive Ge-Si intermixing inside QDs. The cross-section images obtained by TEM (transmission electron microscopy) show that the height of disk-like dots does not exceed 3 nm in the experimental structure. These dots, as well as original *domes*, are characterized by the absence of mirror symmetry due to a difference between the smeared top and sharper bottom of QDs. So, after such overgrowth the localization radius is expected to be comparable with the lateral size of QD.

STM data show a non-homogenous in-plane distribution of *dome*-clusters and the existence of groups of 2-3 closely spaced nanoclusters on the average (Fig. 1). A sufficient tunneling coupling between them allows the electron wave function to spread over the group of QDs and promotes a further increase of the electron localiza-

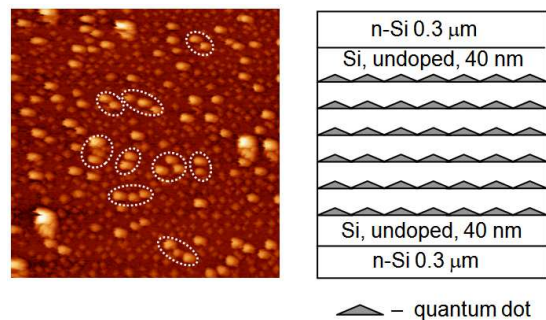


FIG. 1: Right panel: STM of the uncovered sample with two-shaped QDs (*hut*-clusters and *dome*-clusters), $1\ \mu\text{m} \times 1\ \mu\text{m}$ image. Left panel: a schematic structure of investigated sample. The examples of quantum dot groups are indicated by dashed line loops.

tion radius.

Hut-clusters in these structures can not be the centers of localization because the binding energy of electron on such type quantum dots is very small ($\sim 10\text{meV}$).¹¹ Recently, to provide the localization of electrons on *hut*-clusters, the stacked structures with four layers of Ge quantum dots were grown¹². The distances between QD layers were 3 nm, 5 nm, and that resulted in the effective deepening of potential well near *hut*-clusters due to accumulation of strain from different QD layers. In the structure under study the distance between QD layers is 30 nm, then the strain accumulation does not occur.

ESR measurements were performed with a Bruker Elexsys 580 X-band EPR spectrometer using a dielectric cavity Bruker ER-4118 X-MD-5. The samples were glued on a quartz holder, then the entire cavity and the sample were maintained at a low temperature with a helium flow cryostat (Oxford CF935). The needless EPR signal from dangling bonds ($g = 2.0055$) was avoided using the passivation of structures with atomic hydrogen before measurements. To increase the number of registrable spins, the sandwiched sample was prepared. Samples were thinned by acid etching up to $150 - 250\ \mu\text{m}$. After thinning, samples were glued together; finally, the object composed of 4-5 wafers was investigated.

The spin echo measurements were carried out at temperature 4.5 K in resonance magnetic field $H = 3470\text{G}$ (can be slightly varied $\pm 5\text{G}$ depending on resonance conditions) with direction corresponding to the narrowest ESR line width, $\theta = 30^\circ$, where θ is the angle between magnetic field and growth direction of the structure [001]. A two-pulse Hahn echo experiment ($\pi/2 - \tau - \pi - \tau -$ echo) was used to measure T_2 (a detailed explanation can be found in Ref. 13). In order to observe a longitudinal spin relaxation (corresponding time T_1), a different pulse sequence is applied ($\pi - \tau - \pi/2 - T - \pi - T -$ echo). The first π -pulse rotates the magnetization opposite to its thermal equilibrium orientation, where the interaction with the environment causes the spins to relax back to the initial orientation parallel to \mathbf{H} . After time τ , a $\pi/2$ -pulse

followed by another π -pulse is used to observe a Hahn echo. In the first and second type of experiments, the durations of $\pi/2$ and π pulses were 60 ns and 120 ns, respectively; the interpulse time in the second experiment was kept $T = 200$ ns.

II. RESULTS

The ESR spectra measured at different directions of magnetic field are shown in Fig. 2, where $\theta = 0^\circ$ corresponds to the magnetic field applied parallel to the growth direction Z . At $\theta = 0^\circ$ the ESR line is most symmetrical and its shape is close to Gaussian. The line asymmetry becomes more pronounced with the increase of angle θ and the line shape tends to Lorentzian already at $\theta = 10^\circ$. The line shape analysis performed at $\theta = 30^\circ$ is shown in Fig. 3. A careful examination of ESR line shape shows that the ESR line represents the sum of an absorption line (dotted) and a dispersion line (dashed). The rotation of the sample in the magnetic field results in a change of the resonance line width and the resonance field. The orientation dependence of the ESR line width for the structure under study is demonstrated in Fig. 4. When the external magnetic field deviates from the growth direction up to $\theta \approx 30^\circ$, the ESR line width sharply decreases from $\Delta H = 1.9$ Oe to $\Delta H = 1.4$ Oe. A further tilt of the magnetic field leads to the line broadening with maximum $\Delta H = 2.4$ Oe at $\theta = 60^\circ$. For the in-plane magnetic field, the ESR line width is narrowed again down to $\Delta H = 1.8$ Oe. Such nonmonotonic behavior is unusual for electrons in 2D system, and has not been observed up to now.

The angular dependence of g-factor is shown in Fig. 5. At small angles (up to 30°) the g-factor slightly changes nearly $g = 1.9994(5)$. Between $\theta = 30^\circ$ and $\theta = 40^\circ$ the g-factor value jumps to $g = 1.9992$ and remains nearly constant up to $\theta = 90^\circ$.

The data of spin echo measurements performing at $\theta = 30^\circ$, when the most narrow ESR line width is observed, are shown in Fig. 6, 7. According to the results of a two-pulse Hahn echo experiment, the spin echo behavior can be described by superposition of two exponentially decaying functions:

$$M(t) = M_{x,y}^{(1)} \exp(-2\tau/T_2^{(1)}) + M_{x,y}^{(2)} \exp(-2\tau/T_2^{(2)}), \quad (1)$$

where $M(0) = M_{x,y}^{(1)} + M_{x,y}^{(2)}$ is the lateral (in QD plane) magnetization after $\pi/2$ -pulse. The decay parameters give two times of spin dephasing: $T_2^{(1)} \approx 0.26 \mu\text{s}$ and $T_2^{(2)} \approx 1.5 \mu\text{s}$.

The analysis of the inversion signal recovery measured in three-pulse echo experiments shows non-exponential behavior (Fig. 7). The experimental curve can be described by the superposition of two functions:

$$M(t) = M_{0z} - M_z^{(1)} \exp(-\tau/T_1^{(1)}) - M_z^{(2)} \exp(-\tau/T_1^{(2)}), \quad (2)$$

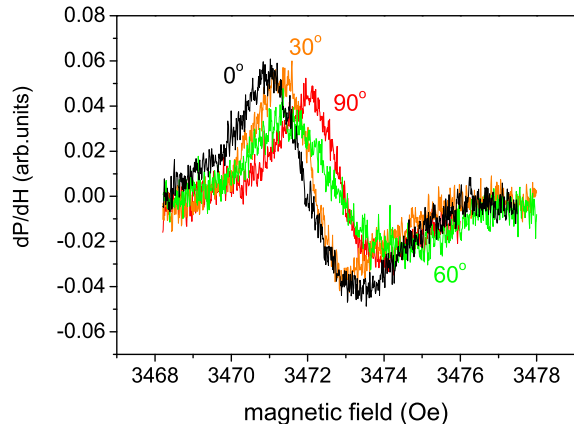


FIG. 2: ESR spectra at different orientations of magnetic field. For $\theta = 0^\circ$ the magnetic field is parallel to the growth direction of the structure [001], $\theta = 90^\circ$ corresponds to magnetic field applied along crystallographic direction [110].

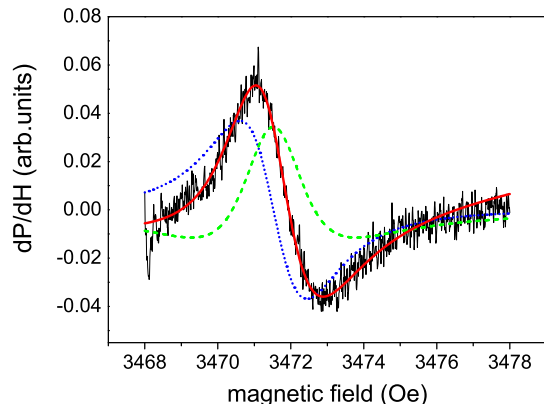


FIG. 3: Analysis of the ESR line shape for $\theta = 30^\circ$. The solid line represents the sum of an absorption line (dotted), and a dispersion line (dashed).

where M_{0z} is the equilibrium magnetization, $M_{0z} = M_{0z}^{(1)} + M_{0z}^{(2)}$, $M_z^{(1,2)} = M_{0z}^{(1,2)} - M_z^{(1,2)}(0)$, $M_z(0) = M_z^{(1)}(0) + M_z^{(2)}(0)$ is the magnetization just after applying of an inverting π -pulse. In correspondence with this equation at the beginning the samples magnetization recovers very fast. After some time the part of spins is returned to an equilibrium state and the recovery rate becomes much slower. The characteristic times obtained by fitting the experimental data are $T_1^{(1)} \approx 2 \mu\text{s}$ and $T_1^{(2)} \approx 35 \mu\text{s}$. All values of spin relaxation times were determined with error $\pm 20\%$.

III. DISCUSSION

To explain the experimental results obtained in the present work, we propose the following model (see Fig. 8).

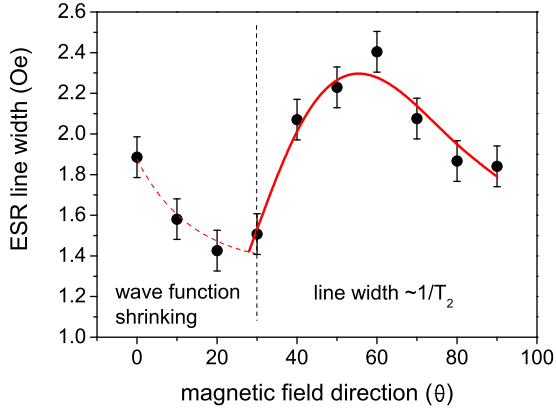


FIG. 4: The angular dependence of ESR line width and theoretical approximation (Eq.6) of this dependence (solid line) for the structure under study. For $\theta = 0^\circ$ the magnetic field is parallel to the growth direction of the structure.

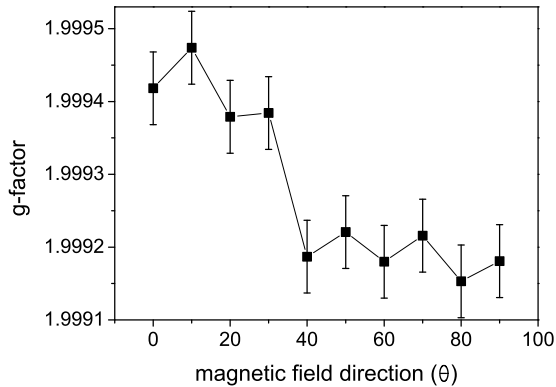


FIG. 5: The angular dependence of electron g-factor for the structure under study. For $\theta = 0^\circ$ the magnetic field is parallel to the growth direction of the structure.

Electrons are suggested to localize mainly in the groups of closely spaced QDs containing 2-3 QDs on the average (see STM data). During overgrowth QDs lose their apex and transform to the disk-like shape QDs. As a result, the electron localization radius can become comparable with QD lateral size. Additional barriers for electrons limiting the electron motion in XY directions in the Si layer arise due to the regions with a nonzero Ge content. These regions are located over the edges along the perimeter of QDs and they are formed following the mechanism of formation of SiGe rings described in Ref.14. Thus, the electron localization radius can be taken about 50 nm for a spatially isolated single QD. In the case of a group of closely spaced QDs the separating SiGe barriers between dots inside the group are absent because of energetically unfavorable positions of

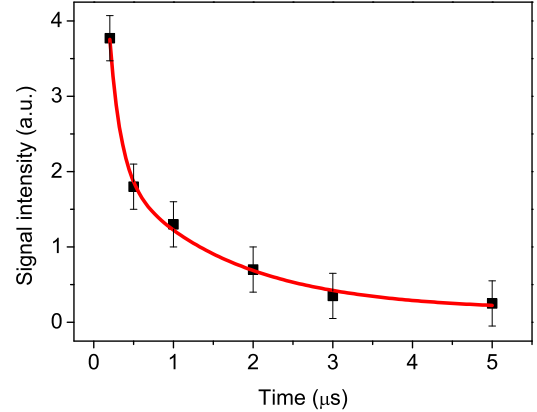


FIG. 6: Results of two-pulse spin echo experiments performed at $\theta = 30^\circ$ (points) and approximation by superposition of two exponential functions, Eq.1 (solid line). Corresponding microwave pulse sequence is $\pi/2 - \tau - \pi - \tau - echo$.

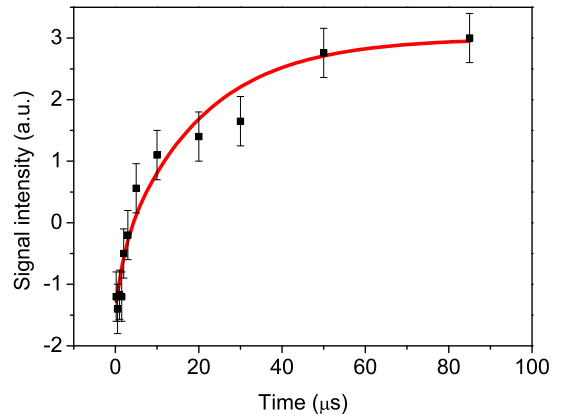


FIG. 7: Amplitude of inversion-recovery signal versus interspike delay τ (symbols are experimental data, solid line is the approximation by Eq.2). Corresponding microwave pulse sequence is $\pi - \tau - \pi/2 - T - \pi - T - echo$. Experiments are performed at $\theta = 30^\circ$.

Ge atoms between QDs due to a high strain.¹⁵ SiGe barriers remain only along the external border of QD groups. Then the electron wave function can spread to the size of the QD group, $l \sim 100 - 150$ nm. Since the confinement of electrons is not too strong, the tails of electron wave functions from different QD groups can be overlapped providing the hopping between QD groups. The external magnetic field applied along the growth direction can sufficiently change the described picture. Magnetic length $\lambda = \sqrt{\hbar/eH}$, in our experimental set up ($H=3470$ Oe), is about 45 nm, that is comparable with the electron localization radius for a single QD. In these conditions, the magnetic field effectively shrinks the tails of electron wave functions, resulting in the enhancement

of electron localization. Thus, the perpendicular magnetic field suppresses the transitions between QD groups and decreases the electron localization radius in the QD group down to the size of an individual QD. Nevertheless, the transitions between QDs inside the groups still persist due to a small distance between QDs. With the deviation of the magnetic field from the growth direction the probability of electron transitions between dots increases and the conductivity in local areas (QD groups) becomes higher. In experiment, this corresponds to the appearance of a noticeable dispersion signal and the enhancement of asymmetry of ESR line (ESR line becomes close to Dysonian line¹⁶). A similar effect was observed for SiGe/Si/SiGe structures with two-dimensional (2D) electron gas.¹⁷

At the same time the increase of the effective electron localization radius causes the averaging of the local magnetic fields induced by nuclear spins and the smoothing of the QD parameter differences within a QD group. As a result, the narrowing of ESR line at the deviation of magnetic field from $\theta = 0^\circ$ to $\theta = 30^\circ$ is observed. The minimum of ESR line width at $\theta = 30^\circ$ indicates that the electron localization radius reaches the size of QD group and the full averaging inside each group takes place. A further increase of the electron localization radius leads to the enhancement of hopping between groups and a decrease of spin lifetime through Dyakonov-Perel spin relaxation mechanism.

The decreasing spin relaxation time affects the ESR line width. From $\theta = 30^\circ$ the broadening due to spin relaxation, $\Delta H \cong 1/T_2$, exceeds the nonhomogeneous broadening and further orientation dependence of ESR line width is controlled by spin relaxation time.

It should be noted that there is one more mechanism which can provide the anisotropy of ESR line width, the relaxation assisted by spin-phonon interaction. This mechanism can be effective due to the lack of phonon bottleneck in our structures with large QD sizes resulting in small confinement energies of electrons. In this case the anisotropy of spin relaxation processes is defined by the shape asymmetry of disk-like QDs. Their lateral size is one order larger than their height, therefore only k_x - and k_y -phonon waves effectively influence the spin. However, the experimentally observed maximum of ESR line width at $\theta = 60^\circ$ cannot be described in the frames of the spin-phonon interaction model,¹⁸ which should provide a monotonic orientation dependence of ESR line width.

Dyakonov-Perel mechanism allows to describe non-monotonic behavior of ESR line width on the assumption of τ_h depending on the magnetic field. This dependence, determined in the frame of the hopping model,¹⁹ can be described as exponential:

$$\tau_h = \tau_0 \exp(\alpha H_z^m), \quad (3)$$

where H_z is the projection of magnetic field to the growth direction; coefficient m can be equal to $m = 1/2$ or $m = 2$ for case of strong or weak magnetic fields. For intermediate fields $\lambda \sim l$ this coefficient can take a value in the

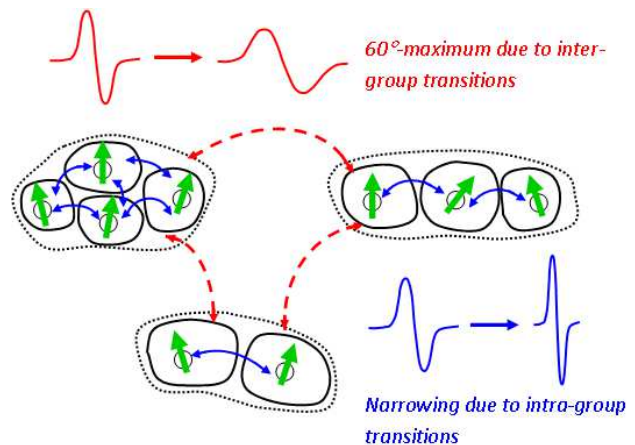


FIG. 8: Illustration of a hopping model for the structure under study. Hopping transitions inside the QD groups provide the narrowing of ESR line with the deviation of magnetic field from $\theta = 0^\circ$ to $\theta = 30^\circ$. Hopping transitions between QD groups provoke the spin relaxation through the spin precession mechanism and give a special orientation dependence of ESR line width in the range of $\theta \in \{30^\circ - 90^\circ\}$.

range of $\{\frac{1}{2} \div 2\}$ (Ref. 19).

Spin relaxation time T_2 in the frames of Redfield theory²⁰ is given by the following expression:

$$\frac{1}{T_2} = \gamma^2 \delta H_y^2 \sin^2 \theta \tau_h + \frac{1}{2T_1}, \quad (4)$$

with

$$\frac{1}{T_1} = \gamma^2 (\delta H_x^2 + \delta H_y^2 \cdot \cos^2 \theta) \frac{\tau_h}{1 + \omega_0^2 \tau_h^2}, \quad (5)$$

where correlation time of spin-orbit field fluctuations τ_c was replaced by hopping time τ_h ; the ω_0 is the Larmor frequency; δH_x , δH_y are the components of effective magnetic field δH .

So, using expression (3) for τ_h , we obtain the following expression describing the orientational dependence of ESR line width:

$$\Delta H = B \exp(A \cos^m \theta) \left(\sin^2 \theta + \frac{1 + \cos^2 \theta}{1 + C \exp(2A \cos^m \theta)} \right), \quad (6)$$

where $B = \gamma \delta H_y^2 \tau_0$, $A = \alpha H^m$, $C = \omega_0^2 \tau_0^2$. The experimental data $\Delta H(\theta)$ in the range of $\theta \in \{30^\circ; 90^\circ\}$ are well approximated by this expression (Fig. 4) with $m = 3/2$, $A = 1.52$, $B = 1.78$, $C = 795.2$. Obtained coefficient m corresponds to the case of intermediate magnetic fields ($\lambda \sim l$) that argues for accepted hopping model with τ_h depending on the magnetic field.

The magnitude of the effective magnetic field δH , estimated from the B coefficient turns out to be ≈ 15 Oe. This value is twice smaller than that determined in our previous work²¹ for *hut* clusters with the aspect ratio $h/l=0.1$. It is known²² that in a QD system the effective

magnetic field depends on h/l , the more the aspect ratio the larger the δH . For QDs under study the aspect ratio is about of ≈ 0.05 , therefore the effective magnetic field proved to be smaller.

The spin echo data are in a good agreement with the proposed model of the existing closed groups of quantum dots being the centers of electron localization in the sample. Experimental spin polarization behavior shows that the spin relaxation occurs in two stages, rapid and slow ones. To understand the origin of this two-stage spin dynamics we simulated the spin relaxation process in the ring-shaped group of quantum dots. Model includes the strong tunneling coupling between quantum dots in the circle. Hopping between any neighboring QDs is permitted with an equal probability for back and forth motion. Each tunneling transition is accompanied by spin rotation on a small fixed angle $\alpha = 0.1$. The direction of the rotation axis is defined by product $[\mathbf{n} \times \mathbf{e}_z]$, where \mathbf{n} -tunneling direction, \mathbf{e}_z -growth direction of QD. The external magnetic field is applied along \mathbf{e}_z and provides the Larmor precession between tunneling events. The time intervals between tunneling events are distributed exponentially with a mean value τ_h . The spin relaxation caused by the interaction with phonons and nuclear spins was not included into the consideration. The transport was simulated by Monte-Carlo method for a different number of QDs in the circle. The results of simulation for the ring constructed of 10 quantum dots are demonstrated in Fig. 9. The two stage spin dynamics is clearly seen. It turned out that this effect depends on the relation between hopping time τ_h and Larmor frequency ω_l . The two-stage dynamics is observed when $\omega_l \tau_h \ll 1$. For example, the data in Fig. 9 were obtained at $\omega_l \tau_h = 0.1$. The first stage of spin relaxation is related to the processes of electron spreading all over the group of QDs. At this stage the loss of spin polarization occurs due to the precession in the effective magnetic field during tunneling between dots. The spin dynamics at the second stage is defined by the phase breaking of Larmor precession during a random walk along the QD ring. Generally speaking, this stage of spin relaxation can be ruled by spin-phonon or hyperfine interaction as well, if one includes them in the consideration. The absence of two-stage dynamics in the case of $\omega_l \tau_h \geq 1$ can be understood by the simple consideration of spin behavior in the frame of reference rotating with Larmor frequency. The randomness of hopping between dots leads to averaging of effective magnetic field ($\langle \delta H \rangle = 0$) and elimination of spin relaxation at the first stage of electron extension over the group of QDs. According to the simulation results, the first rapid stage is characterized by a special relation between the longitudinal and transverse spin relaxation times T_1 and T_2 , usual for 2D system with the absence of mirror symmetry $T_2 \approx 2T_1$. Such relation was obtained by spin echo measurements for 2D electron gas structures²³ and for dense homogeneous QD arrays,⁴ and follows from the in-plane arrangement of fluctuating magnetic fields δH . Also we have verified the presence of

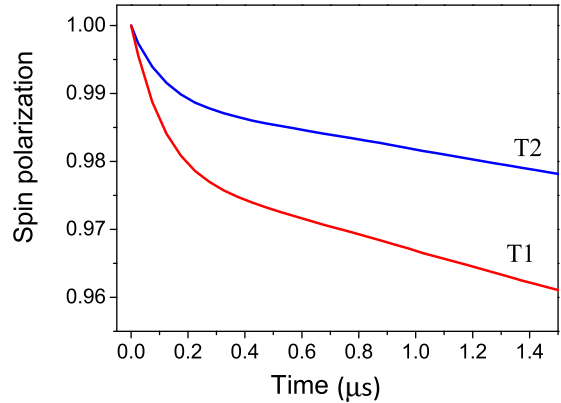


FIG. 9: Results of spin relaxation simulation in a closed ring-shaped group of QD. Number of QDs in the ring - $n = 10$. The hopping time is taken as $\tau_h = 10^{-11}$ s, Larmor frequency was one order smaller $\omega = 10^{10}$ s $^{-1}$. Two stage dynamics is observed.

two-stage spin dynamics in QD clusters with other spatial arrangements, for example, QD lines containing a few dots. The described general features are well preserved with changing only numerical values of T_1 and T_2 .

In experiment on the T_2 -measurements the first stage is characterized by $T_2 \approx 0.26 \mu\text{s}$. Based on the simulation results one can expect the same shortness for T_1 . However, the three-pulse method has limitations on measurements of such short times. The difference between durations of the pulse sequences in T_1 -experiments and T_2 -experiments is comparable with duration of the first rapid stage of spin relaxation that makes difficult the study of the beginning of S_z -relaxation.

The second stage of spin relaxation has the times $T_1 = 2 \mu\text{s}$ and $T_2 = 1.5 \mu\text{s}$. Here, the special relation $T_2 \approx 2T_1$ is not fulfilled because of the presence of some additional spin relaxation mechanisms, for example, Larmor precession phase breaking during a random walk along the QD group or another one. The presence of long living spin polarization with characteristic time $T_1 \approx 35 \mu\text{s}$ is attributed to some stabilization of the S_z -component taking place at the electron movement within a closed QD group. According to the simulation results at a high hopping frequency ($\omega_l \tau_h < 0.01$) the spin polarization after rapid stage is settled at some level depending on parameters of QD groups. In this case, Larmor precession can be neglected, and the sequence of small turnings in Rashba fields can be considered as the effective precession around growth direction Z . In these conditions, the S_z -component is stabilized. In contrast, the transverse component of spin relaxes quickly, then in the experiment we did not observe the rest transverse spin polarization with a long relaxation time.

The orientational dependence of the g -factor allows us to add some details to the considered model. The value

of g-factor $g=1.9994$, within the experimental error, coincides with typical g-factor value for electron states near the conduction band edge in Si.²⁴ The fact that the g-factor remains near this value up to $\theta \approx 30^\circ$ confirms that electron is located in Si regions until this orientation of magnetic field. In other words, the electron increases its localization radius remaining in Si regions. After point $\theta = 30^\circ$, the electron localization radius exceeds the size of QD groups and the g-factor drastically changes to value $g = 1.9992$. Such behavior can be explained by the penetration of electron wave function in SiGe regions surrounding QD groups. The presence of Ge atoms can provide a decrease of the g-factor value.²¹

It should be noted that the same value of electron g-factor was obtained by us in another ESR experiment for the structure with large SiGe nanodisks having diameter 100-150 nm. For this structure we use substrate with specially created nucleation sites to obtain more ordered array of quantum dots. These nucleation sites originated due to strain modulation in the surface layer induced by previously buried QDs. Large *dome*-clusters grown at previous stage at temperature 650° have a good spatial ordering due to a long range elastic interaction between QDs.¹⁵ On this strain-modulated surface we have grown 10 layers of QDs using the same temperature regime as in the structure under study ($T = 550^\circ$ C for QD growth and $T = 500^\circ$ C for overgrowth by Si). However, we reduce the amount of deposited Ge down to 4 ML in each QD layer, and, as result, we obtain a well-ordered array of nanodisks after overgrowth by Si. Thus, we can compare two structures: 1) a non-ordered array with groups of closely spaced QDs and 2) a well-ordered array of nanodisks, one nanodisk instead of one QD group. The average size of QD groups coincides with the characteristic size of nanodisks.

ESR data obtained on the test structure with nan-

odisks confirm the model proposed in this work. ESR signal has isotropic g-factor $g = 1.9992 \pm 0.0001$ and isotropic ESR line width $\Delta H_{pp} \approx 0.4$ Oe. Absolute value of g-factor is the same as in the structure with QD groups at $\theta > 30^\circ$. This can be explained by identical electron localization radius and identical temperature regime of QD creation. The last factor defines the GeSi intermixing and strain in the QD system, which have a high influence on g-factor value. The isotropy of ESR line is explained by the absence of tunneling transitions between nanodisks, which are well ordered in the plane and positioned at an equal (~ 100 nm) distance from each other. Narrowness of ESR line indicates the high efficiency of averaging of nuclear magnetic fields by the electron state with large localization radius and the high uniformity of array of nanodisks (negligible inhomogeneous broadening). In the structure with QD groups the averaging by means of tunneling between dots is not so efficient, then we observe a few times larger ESR line width.

In summary, we demonstrate that the existence of closely spaced QD groups provides the increase of spin relaxation time in QD system. Changing the electron localization radius by external magnetic field allows us to catch the effect of ESR line narrowing and obtain at the special orientation of magnetic field the fourfold increased time T_1 as compared to the recently studied homogeneous QD arrays.

Acknowledgments

This work was supported by RFBR (Grants 11-02-00629-a, 13-02-12105.), SB RAS integration project No. 83 and DITCS RAS project No. 2.5.

* Electronic address: aigul@isp.nsc.ru

¹ I. Žutić, J. Fabian, S. Das Sarma, *Spintronics: Fundamentals and applications*. Rev. Mod. Phys. **76**, 323-410 (2004).

² D. Loss and D. P. DiVincenzo, Phys. Rev. A **57**, 120 (1998); B. E. Kane, Nature (London) **393**, 133 (1998).

³ M. Kroutvar, Y. Ducommun, D. Heiss, M. Bichler, D. Schuh, G. Abstreiter, J. Finley, Nature **432**, 81 (2004).

⁴ A. F. Zinovieva, A. V. Dvurechenskii, N. P. Stepina, A. I. Nikiforov, A. S. Lyubin, L. V. Kulik, Phys. Rev. B. **81**, 113303 (2010)

⁵ Y. A. Bychkov and E. I. Rashba, J. Phys. C **17**, 6039 (1984).

⁶ M. D'yakonov, V. Perel', Sov. Phys. Solid State **13**, 3023 (1972).

⁷ A. F. Zinovieva, A. V. Nenashev, A. V. Dvurechenskii, Proceedings of 18th International Symposium "Nanostructures: Physics and Technology", St. Petersburg, 2010, p. 191.

⁸ B. I. Shklovskii, Phys. Rev. B **73**, 193201 (2006).

⁹ R. I. Dzhiboev, K. V. Kavokin, V. L. Korenev, M. V.

Lazarev, B. Ya. Meltser, M. N. Stepanova, B. P. Zakharchenya, D. Gammon, and D. S. Katzer, Phys. Rev. B **66**, 245204 (2002)

¹⁰ Stranski, I. N., and L. Krastanow, 1938, Sitzungsber. Akad. Wiss. Wien, Math.-Naturwiss. Kl., Abt. 2B **146**, 797.

¹¹ A. I. Yakimov, A. V. Dvurechenskii, N. P. Stepina, A. V. Nenashev, A. I. Nikiforov, Nanotechnology, **12**, 441 (2001).

¹² A. I. Yakimov, A. V. Dvurechenskii, A. I. Nikiforov, A. A. Bloshkin, A. V. Nenashev, V. A. Volodin, Phys. Rev. B, **73**, 115333 (2006).

¹³ A. Schweiger and G. Jeschke, *Principles of Pulse Electron Paramagnetic Resonance* (Oxford University Press, Oxford, 2001).

¹⁴ C.-H. Lee, Y.-Y. Shen, C. W. Liu, S. W. Lee, B.-H. Lin, and C.-H. Hsu, Applied Physics Letters **94**, 141909 (2009)

¹⁵ G. Capellini, M. De Seta, F. Evangelisti, V. A. Zinovyev, G. Vastola, F. Montalenti, Leo Miglio, Phys. Rev. Lett. **96**, 106102 (2006)

¹⁶ F. J. Dyson, Phys. Rev., **98**, 349 (1955).

- ¹⁷ Z. Wilamowski, W. Jantsch, Phys. Rev. B **69**, 035328 (2004).
- ¹⁸ A. F. Zinov'eva, A. V. Nenashev, A. V. Dvurechenskii, JETP Letters **82**, 302 (2005).
- ¹⁹ B. I. Shklovskii, A. L. Efros, *Electronic Properties of Doped Semiconductors*, (Berlin, Springer, 1984).
- ²⁰ C.P. Slichter, *Principles of Magnetic Resonance* (Springer-Verlag, Berlin, Heidelberg, New York, 1978).
- ²¹ A. F. Zinovieva, A. V. Dvurechenskii, N. P. Stepina, A. S. Deryabin, A. I. Nikiforov, R. M. Rubinger, N. A. Sobolev, J. P. Leitaó, M. C. Carmo, Phys. Rev. B **77**, 115319 (2008)
- ²² A. F. Zinovieva, A. V. Nenashev, A. V. Dvurechenskii, Phys. Rev. B **71**, 033310 (2005).
- ²³ A. M. Tyryshkin, S. A. Lyon, W. Jantsch, and F. Schäffler, Phys. Rev. Lett. **94**, 126802 (2005).
- ²⁴ C. F. Young, E. H. Poindexter, G. J. Gerardi, W. L. Warren, D. J. Keeble, Phys. Rev. B **55**, 16245 (1997).